

Globular cluster candidates in the Sagittarius dwarf galaxy

ANDRÉS E. PIATTI^{1,2}

¹*Instituto Interdisciplinario de Ciencias Básicas (ICB), CONICET-UNCUYO, Padre J. Contreras 1300, M5502JMA, Mendoza, Argentina*

²*Consejo Nacional de Investigaciones Científicas y Técnicas (CONICET), Godoy Cruz 2290, C1425FQB, Buenos Aires, Argentina*

ABSTRACT

Recently, new Sagittarius (Sgr) dwarf galaxy globular clusters were discovered, which opens the question on the actual size of the Sgr globular cluster population, and therefore on our understanding of the Sgr galaxy formation and accretion history onto the Milky Way. Based on *Gaia* EDR3 and SDSS IV DR16 (APOGEE-2) data sets, we performed an analysis of the color-magnitude diagrams (CMDs) of the eight new Sgr globular clusters found by Minniti et al. (2021b) from a sound cleaning of the contamination of Milky Way and Sgr field stars, complemented by available kinematic and metal abundance information. The cleaned CMDs and spatial stellar distributions reveal the presence of stars with a wide range of cluster membership probabilities. Minni 332 turned out to be a younger (< 9 Gyr) and more metal-rich ($[M/H] \gtrsim -1.0$ dex) globular cluster than M54, the nuclear Sgr globular cluster, as could also be the case of Minni 342, 348, and 349, although their results are less convincing. Minni 341 could be an open cluster candidate (age < 1 Gyr, $[M/H] \sim -0.3$ dex), while the analyses of Minni 335, 343, and 344 did not allow us to confirm their physical reality. We also built the Sgr cluster frequency (CF) using available ages of the Sgr globular clusters and compared it with that obtained from the Sgr star formation history. Both CFs are in excellent agreement. However, the addition of eight new globular clusters with ages and metallicities distributed according to the Sgr age-metallicity relationship turns out in a remarkably different CF.

Keywords: galaxies: individual: Sagittarius – galaxies: star clusters: general – techniques: photometric

1. INTRODUCTION

The study of the population of old globular clusters in the Sagittarius (Sgr) dwarf galaxy has recently gained a renewed strength from the availability of new kinematic, optical and infrared photometric data sets (e.g. Alfaro-Cuello et al. 2019; Bellazzini et al. 2020; Arakelyan et al. 2021; Minniti et al. 2021a). We here revisited the recent work by Minniti et al. (2021b) who discovered eight globular clusters in the main body of the Sgr dwarf galaxy. Their findings rely on the identification of stellar overdensities in the *Gaia* EDR3 database (Gaia Collaboration et al. 2016, 2020), composed of stars with proper motions within ± 1 mas/yr from the mean values of the nuclear Sgr globular cluster M54’s proper motions. From all the visually identified overdensities with sizes between $1'$ and $2'$, they chose eight whose

color-magnitude diagrams (CMDs) resemble those of Sgr globular clusters. They mentioned that the discovered globular clusters are more metal-rich than M54, because of their redder CMD red giant branches match that of the metal-rich Sgr field population.

The mean $[M/H]$ values for Sgr old globular clusters (ages $\gtrsim 11$ Gyr) are smaller than ~ -1.2 dex (e.g. Kruijssen et al. 2019), similarly to the majority of ancient Milky Way globular clusters born in satellite galaxies (Kruijssen et al. 2020). There are very few satellite globular clusters more metal-rich than ~ -1.0 dex, and all of them are younger than ~ 9 Gyr. Particularly, the Sgr dwarf galaxy globular clusters Terzan 7 and Whiting 1 ($[M/H] \sim -0.6$ dex) have ages that coincide with the time of accretion onto the Milky Way (7 ± 1 Gyr). The Sgr star formation history modeled by Law & Majewski (2010) from N-body simulations and that traced by de Boer et al. (2015) from SDSS data show that the Sgr age-metallicity relationship exhibits two peaks, at ~ 12 Gyr and ~ 7 Gyr, with mean $[M/H]$ values of ~ -1.5 dex

and ~ -0.5 dex, respectively. The star formation rate at the second peak is nearly half or less than that of the earliest formation epoch. We note that the younger peak can be related to bursting formation episodes triggered during the infall of Sgr onto the Milky Way.

The number of globular clusters discovered by Minniti et al. (2021b) is several times that of the Sgr metal-rich globular cluster population, so that they challenge the Sgr globular cluster frequency (number of clusters per time unit) and our knowledge about the Sgr star formation history. An alternative interpretation of Minniti et al. (2021b)'s results is that they are dealing with projected stellar fluctuations along the line-of-sight, whose proper motions are within ± 1 mas/yr from the M54's proper motions (see, figure 4 in Bellazzini et al. 2020). We note that the CMDs used to infer the existence of new globular clusters were not cleaned from field star contamination, but filtered from the proper motion of M54. It is readily possible to get a CMD of the composite stellar population of a nearby galaxy with stars moving with the same proper motions that resembles that of an old single population. If this were the case, then, it would be straightforward to reconcile the redder red giant branches of the discovered globular clusters with the composite projected field population, with metallicities and ages that fully agree with the observed Sgr metal-rich field population.

In this work, we analyze optical CMDs of the eight globular clusters discovered by Minniti et al. (2021b) and conclude that similar CMDs could be built considering the stellar overdensities of the Sgr composite field population. Hence, this work aims at cleaning the new Sgr globular cluster CMDs from field star contamination to assess their nature as genuine physical aggregates (see, also Minniti et al. 2021a). Section 2 describes the data sets used and the method applied to clean the cluster CMDs from the star field contamination. Section 3 deals with the analysis of the cleaned CMDs and of the Sgr cluster frequency in the context of the Sgr age-metallicity and star formation history.

2. DATA HANDLING

We used the *Gaia* EDR3¹ database to build CMDs for the new globular clusters cleaned from field star contamination. We retrieved parallaxes (ϖ), proper motions in right ascension (pmra) and declination (pmdec), excess noise (`epsi`), the significance of excess of noise (`sepsi`), and *G*, *BP*, and *RP* magnitudes for stars located within a radius of $10'$ from the globular clusters' centers. In order to monitor the contamination of field stars in the

globular clusters' CMDs, we retrieved information for circular areas much larger than the globular cluster sizes. In the subsequent analysis, we adopted a circular region of radius $3'$ centered on the globular clusters, for comparison purposes with Minniti et al. (2021b), at the distance of Sgr (26.5 kpc), the scale is $2' = 15$ pc's CMDs. For each globular cluster, we employed six adjacent star field regions of equal globular cluster area distributed around the cluster region, as depicted in Fig. 1. As shown by Minniti et al. (2021b), interstellar extinction seems to be fairly uniform and small at the relatively high southern Galactic latitudes of Sgr ($b < 10^\circ$), so that it does not play any role in the observed variations of the stellar density.

The contamination of field stars plays an important role when dealing with star cluster CMDs, because it is not straightforward to consider a star as a cluster member only on the basis of its position in that CMD. The six surrounding star fields of Fig 1 are thought to be placed far from the globular cluster field, but not too far from it as to become unsuitable as representative of the star field projected along the line-of-sight of the globular cluster. Frequently, it is assumed that the stellar density and the distribution of magnitudes and colors of stars in these star fields are similar to those of field stars located along the line-of-sight of the globular cluster. However, even though the globular cluster is not projected onto a crowded star field or is not affected by differential reddening, it is highly possible to find differences between the astrophysical properties of the surrounding star fields and the globular cluster. Fig. 1 illustrates the stellar distribution in the field of Minni 332, one of the new globular clusters, using all the stars retrieved from *Gaia* EDR3 with *G*, *BP*, and *RP* photometry, and that filtered using proper motions within ± 1 mas/yr from the M54's proper motions (pmra= -2.680 ± 0.026 mas/yr, pmdec= -1.387 ± 0.025 mas/yr; Helmi et al. 2018; Vasiliev & Baumgardt 2021). The latter comprises the stars used by Minniti et al. (2021b) to build the corresponding CMD and to infer the existence of a globular cluster. Thus, by using the same database and selection criteria employed by Minniti et al. (2021b) we could compare their results with those derived in this work. Bearing in mind the above considerations, we decided to clean the star field contamination in the globular cluster CMDs filtered by the M54's proper motion by using, at a time, the six different devised star field areas shown in Fig. 1.

The decontamination of the globular cluster CMDs comprises three main steps, namely: i) to properly deal with each of the six star fields by considering the observed distribution of their stars in magnitude and color; ii) to reliably subtract the star fields from the globu-

¹ <https://archives.esac.esa.int/gaia>.

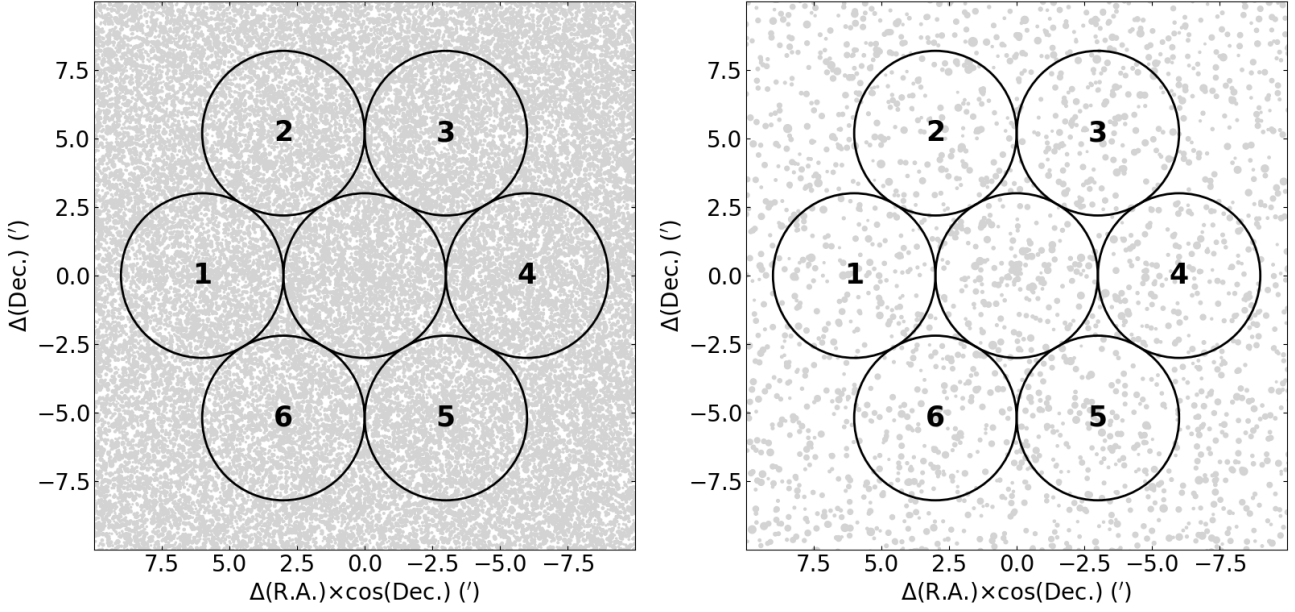


Figure 1. Schematic charts centered on Minni 332 with all stars retrieved from *Gaia* EDR3 with G , BP and RP photometry (left panel), and that for stars with proper motions within ± 1 mas/yr from the M54's proper motion (right panel). The size of the symbols is proportional to the G brightness. Six labeled star field circles distributed around the globular cluster circle are drawn. The radius of each circle is $3'$.

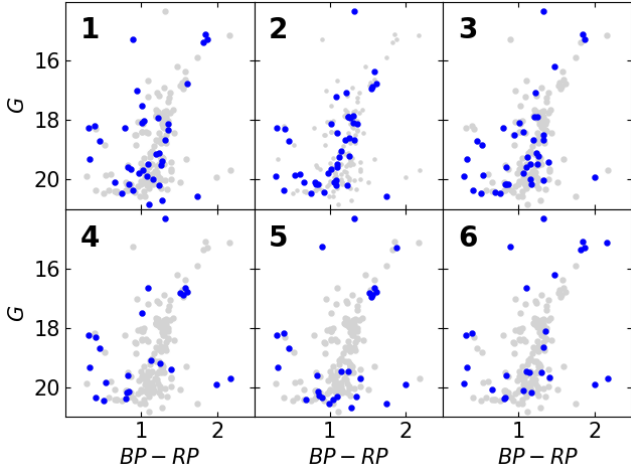


Figure 2. color-magnitude diagrams of Minni 332. Grey symbols represent all the measured stars in the *Gaia* EDR3 database with proper motions within ± 1 mas/yr from the M54's proper motions, located within a circle of $3'$ in radius. Blue symbols represent the stars that remained unsubtracted after the CMD cleaning procedure. The star field used to decontaminate the star cluster CMD is indicated at the top-left margin (see also Fig. 1).

lar cluster CMD (one surrounding star field at a time) and, iii) to assign membership probabilities to stars that were kept unsubtracted in the resulting cleaned globular cluster CMDs. Stars with relatively high membership probabilities can likely be cluster members, if they

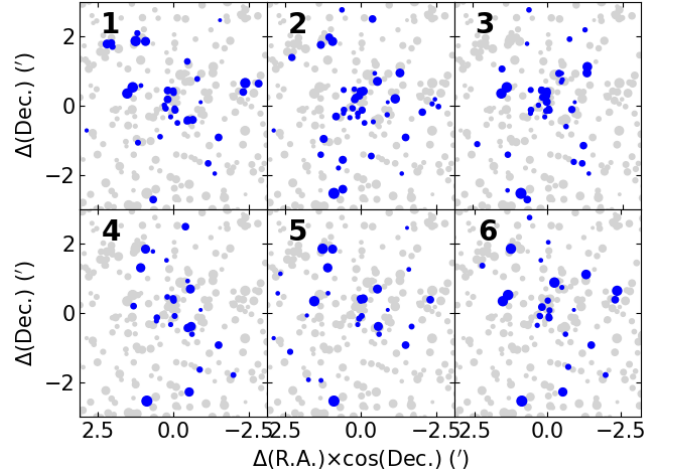


Figure 3. Chart of the stars in the field of Minni 332 with proper motions within ± 1 mas/yr from the M54's proper motion (grey symbols). Blue symbols represent the stars that remained unsubtracted after the CMD cleaning procedure. The size of the symbols is proportional to the G brightness of the star. The star field used to decontaminate the star cluster CMD is indicated at the top-left margin (see also Fig. 1).

are placed along the expected globular cluster CMD sequences. We refer the readers to [Piatti & Bica \(2012\)](#), who devised the above procedure, which was satisfactorily applied in cleaning CMDs of star clusters projected toward crowded star fields (e.g., [Piatti 2017a](#),

and references therein) and affected by differential reddening (e.g., Piatti 2018a, and references therein). The method has also proved to be successful in uncovered tidal tails around Milky Way globular clusters (e.g. Piatti & Fernández-Trincado 2020), in revealing the nature of Large Magellanic Cloud age gap cluster candidates (Piatti 2021), among others.

We subtracted from a globular cluster CMD a number of stars equal to that in a surrounding star field, and repeated the star subtraction for the six devised star fields (see Fig. 1), separately, one at a time. The distribution of magnitudes and colors of the subtracted stars from the globular cluster needs in addition to resemble that of the star field. The method consists in defining boxes centered on the magnitude and color of each star of the star field CMD, then to superimpose them on the globular cluster CMD, and finally to choose one star per box to subtract. With the aim of avoiding stochastic effects caused by very few field stars distributed in less populated CMD regions, appropriate ranges of magnitudes and colors around the CMD positions of field stars were used. Thus, it is highly probable to find a star in the globular cluster CMD with a magnitude and a color within those box boundaries. In the case that more than one star is located inside that delimited CMD region, the closest one to the center of that (magnitude, color) box is subtracted. In the present work, we used initial boxes of $(\Delta G, \Delta(BP - RP)) = (1.0 \text{ mag}, 0.5 \text{ mag})$ centered on the $(G, BP - RP)$ values of each field star.

In practice, for each field star, we first randomly selected the position of a box of $0.5'$ a side inside the globular cluster field where to subtract a star. If no star is found in the selected spatial box, we repeated the selection of a box a thousand times, otherwise we enlarged the box size in steps of $0.5'$ a side, to iterate the process. We then looked for a star with $(G, BP - RP)$ values within a box described above. If no star in the globular cluster field with a magnitude and a color similar to $(G, BP - RP)$ is found after a thousand iterations, we do not subtract any star for that $(G, BP - RP)$ values. The same procedure was applied for all the stars in each surrounding star field. Figure 2 illustrates the different results of the decontamination of field stars when the different six star fields (see Fig. 1) are used, separately. As can be seen, the different resulting cleaned globular cluster CMDs (blue points) show distinct groups of stars, depending on the surrounding star field used, which suggests that differences in the astrophysical properties of the composite star field population do exist. If stars in the six devised star field regions showed a uniform distribution of stars in magnitude and color, all the resulting cleaned CMDs should

look similar. The spatial distribution of the stars that were kept unsubtracted is shown in Fig. 3. From Figs. 2 and 3 is readily visible that the stars that have survived the cleaning procedure are not spatially distributed inside a radius of $\sim 1'-2'$ (the size of the selected objects; Minniti et al. 2021b), nor they unquestionably follow the expected sequences in the star cluster CMD either. This means that those stars could also represent fluctuations in the stellar density along the line-of-sight of the composite stellar field population.

We finally assigned a membership probability to each star that remained unsubtracted after the decontamination of the globular cluster CMD. Because the stars in the cleaned CMDs vary with respect to the star field employed (see the distribution of blue points in Figs. 2 and 3), we defined the probability P (%) = $100 \times N/6$, where N represent the number of time a star was not subtracted during the six different CMD cleaning executions. P reflects the number of times a star appears in Figs. 2 and 3, i.e., a star that was not subtracted while using different surrounding fields as reference. Hence, a star with $P = 100$ is a star that kept unsubtracted all the cleaning runs with six different reference star fields. It has survived even though the observed variations of the star properties (magnitude and color distributions) in the different six star fields. For this reason, it has the highest chance to contribute to the intrinsic features of the cleaned CMD. A star with $P = 16.67$ is that that survived once from six different cleaning executions, meaning that its magnitude and color are frequently found in the surrounding field population. With that information on hand, we built Fig. 4, which shows the spatial distribution and the CMD of all the measured stars with proper motions within $\pm 1 \text{ mas/yr}$ from the M54's proper motion located in the field of the new globular clusters. Stars with different P values were plotted with different colors.

We additionally applied the decontamination procedure to any of the six surrounding star fields using the remaining ones as reference star fields. We found that the resulting cleaned spatial stellar distributions and CMDs do not contain stars with $P > 16.67$, which means that the residuals of the cleaning technique are negligible (see Piatti et al. 2021, where details on the performance of the cleaning procedure are detailed). In order to illustrate how the applied cleaning technique is expected to work in the case of a known globular cluster, we chose M54 as a test example. The cluster is at least as large as $\sim 10'$ in radius (de Boer et al. 2019; Fernández-Trincado et al. 2021, and references therein), so that we cleaned the field star contamination within a circle of that radius centered on the cluster. Six equal cluster areas were

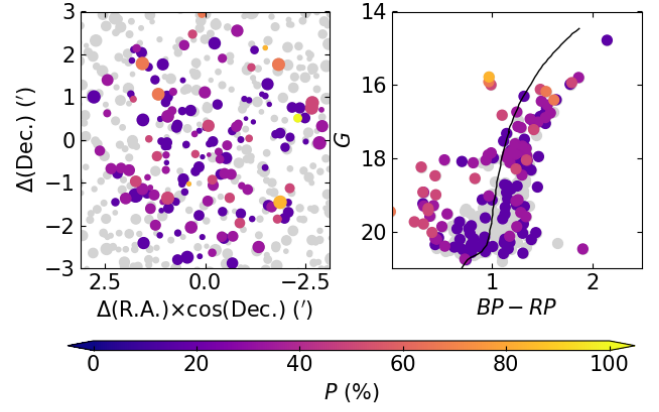
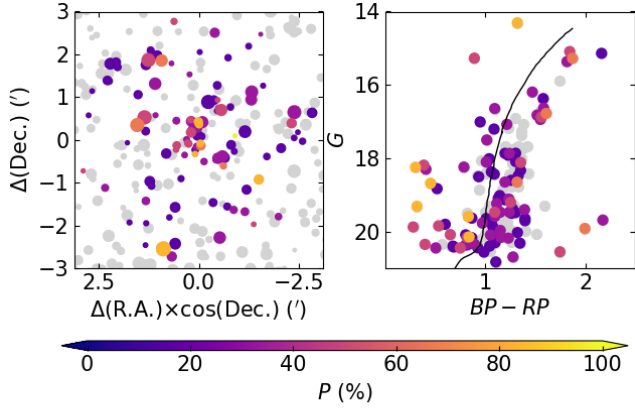


Figure 4. Chart of the stars in the field of Minni 332 with proper motions within ± 1 mas/yr from the M54’s proper motions (left panel), and the respective CMD (right panel), drawn with grey symbols. The size of the chart’s symbols is proportional to the G brightness of the star. colored symbols in both panels represent the stars that remained un-subtracted after the CMD cleaning procedure, color-coded according to the assigned membership probabilities (P). A theoretical isochrone (Bressan et al. 2012) for the age and metallicity of M54 (Kruijssen et al. 2019) is superimposed onto the CMD with a black line.

Figure 4. continued: Minni 341.

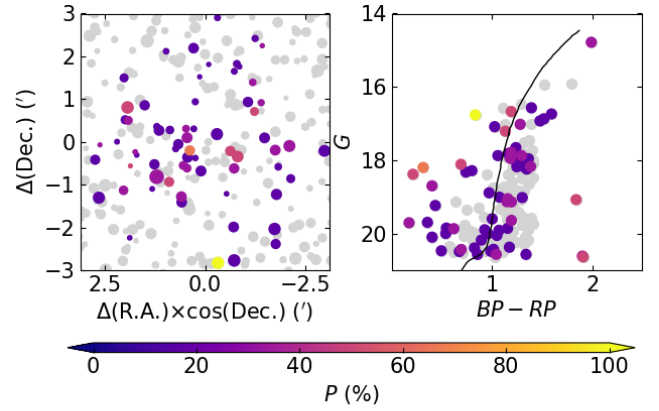


Figure 4. continued: Minni 342.

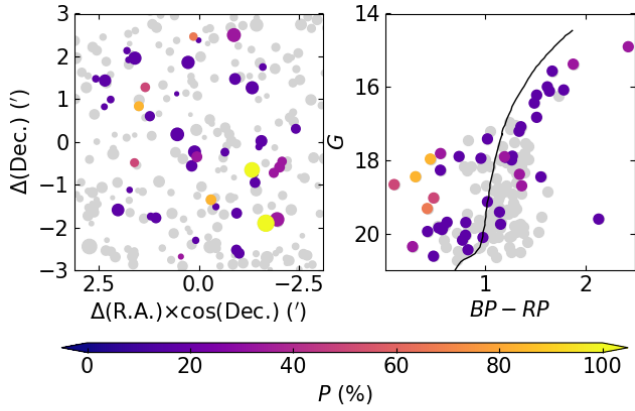


Figure 4. continued: Minni 335.

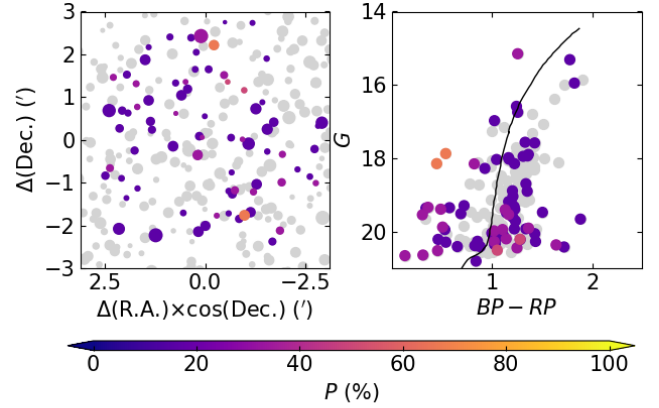


Figure 4. continued: Minni 343.

chosen around M54 as described above as reference star fields. The charts and cleaned CMD color-coded according to the resulting membership probabilities are depicted in Fig. 5.

3. ANALYSIS AND DISCUSSION

3.1. Color-magnitudes diagrams

A close inspection of Fig 4 (both panels) should help us to assess on the existence of new globular clusters.

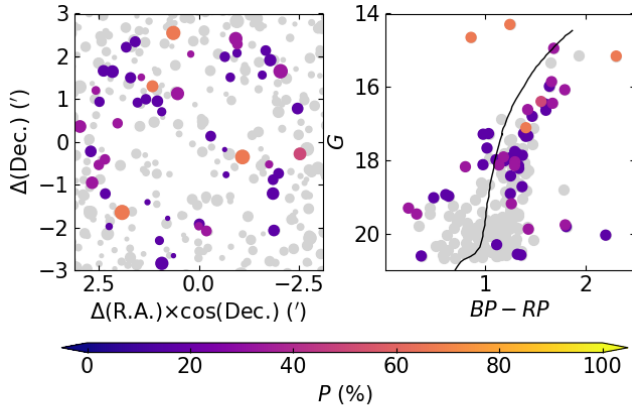


Figure 4. continued: Minni 344.

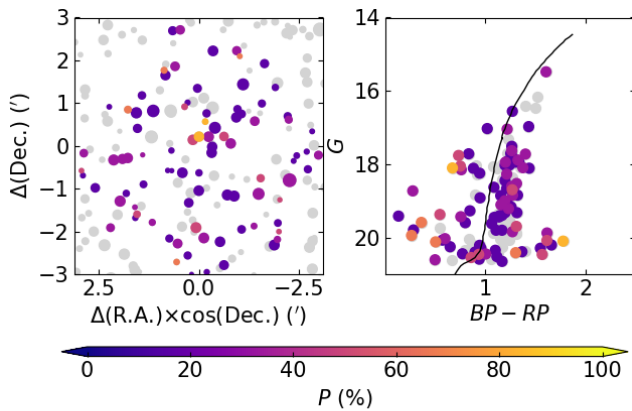


Figure 4. continued: Minni 348.

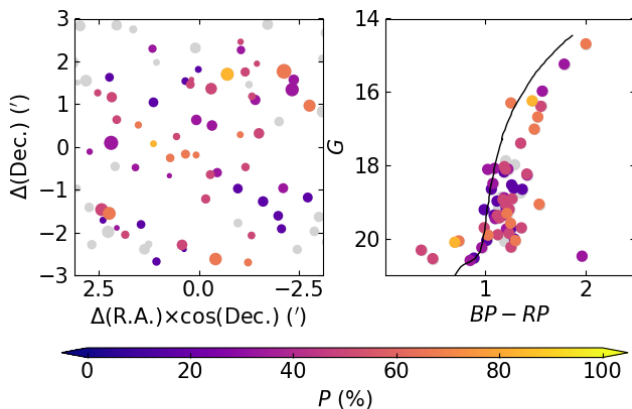


Figure 4. continued: Minni 349.

Note that colored stars are those that have passed at least one cleaning execution and have membership probabilities in the range $0 < P$ (%) ≤ 100 . A low P value arises when a star has been removed several times after the six independent cleaning executions. This means that their magnitude and color are similar to those of the field stars, and that the number of those stars in the cluster region is similar to that in the reference star field. In order to confirm a genuine physical system we focused on those with $P > 50\%$ in the schematic spatial distribution and in the CMD, simultaneously. If these stars form a concentrated group (a compact spatial overdensity) and are distributed along the known CMD globular cluster sequences, we can be dealing with a real aggregate. This seems to be the case of Minni 332: the star concentration is visible, and some hint for a red giant branch is also recognized; there are some high P value stars also scattered in the CMD, as expected because of the statistical nature of the cleaning procedure. Because red giant stars with $P > 50\%$ are redder than those of M54, Minni 332 should be a more metal-rich globular cluster. For comparison purposes we superimposed to Fig. 4 (right panels) a theoretical isochrone (Bressan et al. 2012) for the age and metallicity of M54 (see, Table A1 in Kruijssen et al. 2019).

We used this particular isochrone as a starting point based on Minniti et al. (2021b)'s results that the eight objects are real Sgr ancient globular clusters. If this were the case, the positions of their respective red giant branches would mostly differ in color, in such a way that the redder the color the more metal-rich the globular cluster for a fixed magnitude level (Piatti et al. 2017, and references therein). Ages of old globular clusters with red giant branches whose colors, for a fixed magnitude, correlate with their metallicities are larger than ~ 6 Gyrs (Ordoñez & Sarajedini 2015). Therefore, at first glance, the ages of confirmed old globular clusters should be in that age range. However, the Sgr age-metallicity relationship imposes some constraints for the globular clusters' ages, depending on the clusters' metallicity (Kruijssen et al. 2020). Because we are interested in confirming the physical reality of these objects as old Sgr globular clusters, we assumed that they are at the Sgr distance and share the Sgr age-metallicity relationship.

For Minni 335, 343, and 344, it is hardly possible to identify a spatial concentration of stars with $P > 50\%$ and the few ones with such P values do not follow any expected globular cluster sequence in the respected cleaned CMD. The field of Minni 341 shows an enhancement of stars with respect to that in the reference star fields, because many stars with $P > 0\%$ are

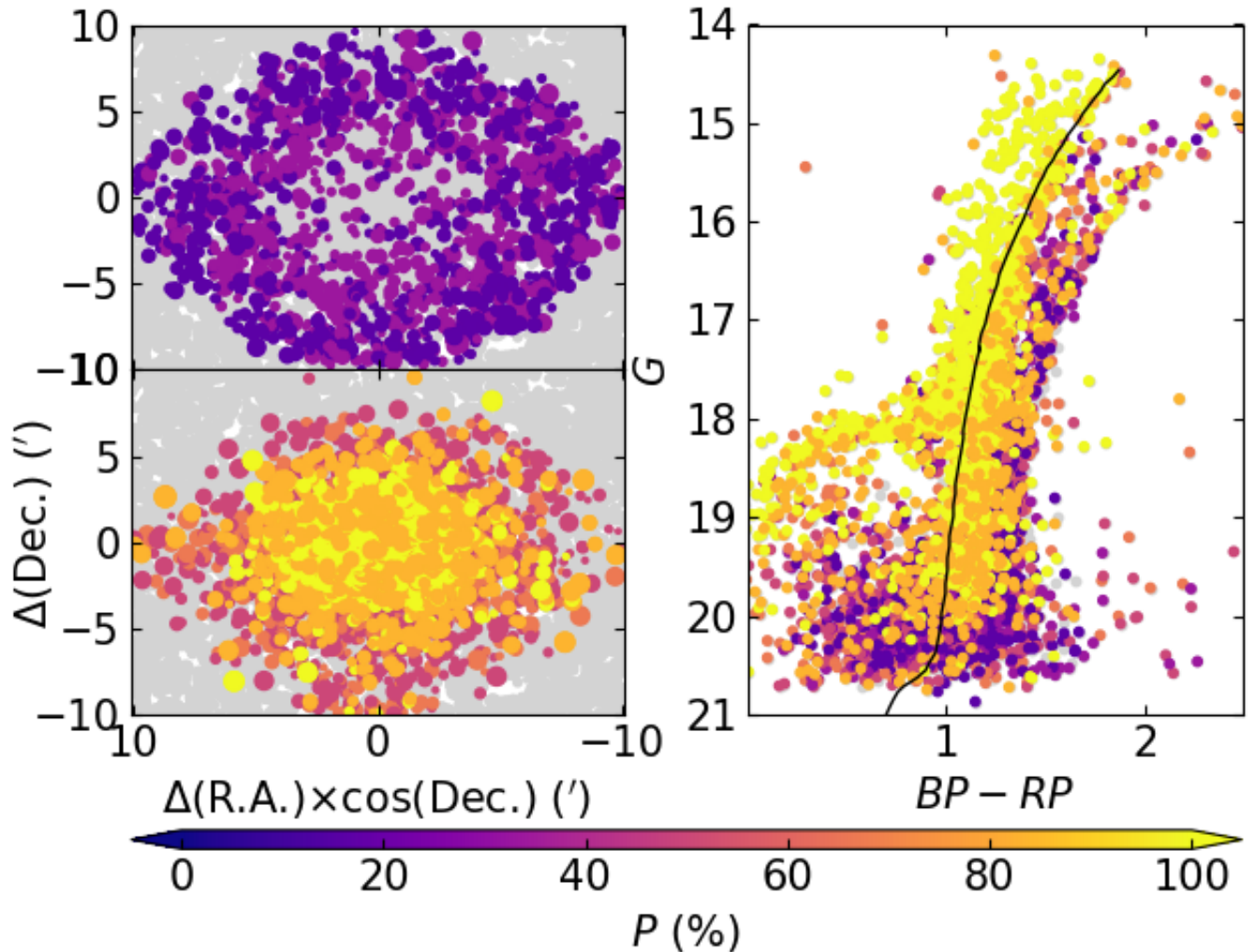


Figure 5. *Left panels:* Charts for different membership probability regimes of the stars in a circle of radius $10'$ centered on M54; they are aimed at avoiding superposition. The size of the symbols is proportional to the G brightness of the star. *Right panel:* CMD of M54 with membership probabilities that highlight the old and metal-poor cluster population. A theoretical isochrone (Bressan et al. 2012) for the cluster age and metallicity (Kruijssen et al. 2019) is superimposed with a black line.

seen with colored symbols. However, their distribution in the CMD suggests the existence of an upper Main Sequence with a turnoff point at $G \sim 19.0$ mag, and some red giants at $G \sim 16.0$ mag, which could resemble a much younger and extended star cluster. Minni 342 and 348 exhibit some concentration of stars with $P > 50\%$ that occupy CMD regions where we expect to see asymptotic and horizontal branch stars, with no strong signature for another CMD cluster feature. Finally, Minni 349 caught our attention because the spatial distribution of the stars does not show any clear concentration, but most of them have $P > 50\%$ distributed along a red giant branch.

As expected, the stars with assigned P values distributed along the Sgr composite star field CMD populate its observed sub-giant and red giant branches, its red clump and horizontal branch, respectively. Note

that, because of the distance of the Sgr dwarf galaxy, they can mimic the CMD feature of a real globular cluster. However, if a genuine globular cluster existed, its stellar populations should differentiate from those of the composite star field, not only as a spatially concentrated excess of stars, but also from the representative age and metallicity of the composite star field. When both conditions are met, the cleaning procedure leaves these stars unsubtracted, and hence, assigns a high membership probability. The cleaning method removes randomly from the cluster field the same number of stars found in the adopted star field, thus preserving any stellar over-density, while subtracts from the cluster CMD stars with magnitude and color distributions similar to those of the field, thus keeping the cluster CMD features. If a globular cluster had an age and a metallicity similar to the composite star field, the resulting cleaned CMD would

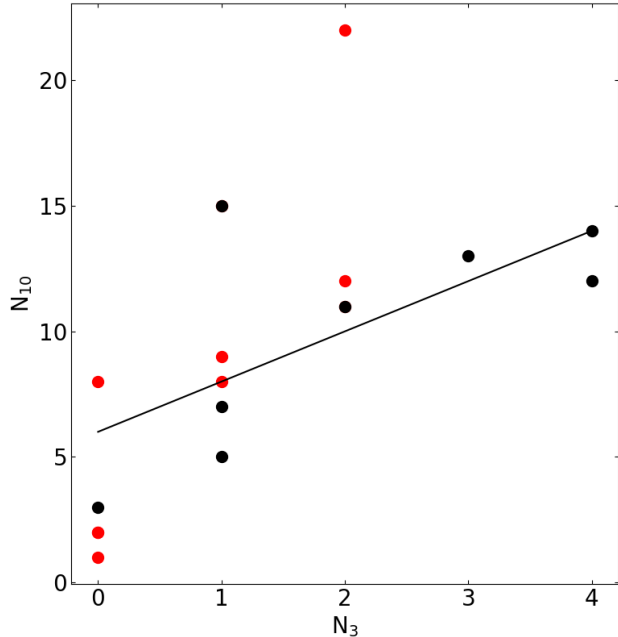


Figure 6. Relationship between the number of RR Lyrae stars counted by Minniti et al. (2021b, Table 1) inside cluster circles of $3'$ (N_3) and $10'$ (N_{10}) of radius. Black and red symbols represent new globular clusters and Sgr fields, respectively. The solid line represents the linear fit to the eight black points.

reveal it as an excess of stars spatially concentrated, distributed along the observed CMD field features and with high P values.

Apparent spatial concentrations of stars are visible in the field of Minni 332, 342 and 348 (see Fig. 4). They can be encircled inside a radius of $\sim 1'$. We note that the circles with radii of $3'$ used by Minniti et al. (2021b) to build the observed CMDs have added some negligible amount of field stars to the constructed CMDs. Likewise, they counted RR Lyrae stars within $3'$ (N_3) and $10'$ (N_{10}) from the cluster circle centers to support the existence of globular clusters. We note however that based only on the positions in the sky, RR Lyrae stars located inside the cluster field could either belong to the cluster or to the field, so that the sole numbers of RR Lyrae stars would not seem enough to conclude on the existence of a real globular cluster. Indeed, we found a linear relationship between the number of RR Lyrae stars counted by Minniti et al. (2021b, see their Table 1) inside $3'$ and $10'$, as follows: $N_{10} = (2.0 \pm 0.8)N_3 + (6.0 \pm 2.0)$, rms = 3.2, and correlation=0.7 (see Fig. 6), which reflects the increase expected from a RR Lyrae population belonging to Sgr field population. For a globular cluster with $1'$ - $2'$ of radius (Minniti et al. 2021b), the number density of cluster RR Lyrae stars should decrease from the cluster radius outwards.

Fig. 5, left panel, shows that inner regions in M54 are mostly populated by stars with membership probabilities higher than $\sim 70\%$, while the analyzed outer regions are dominated by the presence of stars also found in the reference star fields ($P < 20\%$). Because of crowding effects in the *Gaia* EDR3 data sets stars with low P values are not seen in the cluster core. They belong to the faint end of the *Gaia* EDR3 database, where photometry completeness in the cluster core is lower. Nevertheless, their low P values suggest that they are likely Sgr field stars. We split the cleaned spatial distribution in Fig. 5 on purpose in order to highlight where highly probable members are distributed. We note that the purpose of the cleaning procedure is to remove any field star signature from the cluster CMD, so that its cluster features can be clearly recognized. For this reason, a complete cluster photometry is not mandatory, as it is the case when building surface density profiles (Monaco et al. 2005; Bellazzini et al. 2008; Ibata et al. 2009). The resulting cleaned cluster CMD clearly distinguishes the red giant and horizontal branches of M54 and those of the Sgr more metal-rich field populations. Note that some M54 stars ($P > 70\%$) also populate the metal-rich red giant branch, which reflect the existence of multiple populations in this globular cluster. According to Alfaro-Cuello et al. (2019), M54 harbours three main stellar populations of 13.0, 4.5-6.0, and 0.9 Gyr with metallicities of -1.6, -0.4 and 0.5 dex, respectively; the red giant branches of the intermediate-age and young stellar populations being nearly superimposed. The resulting cleaned CMD of M54 with metal-poor and metal-rich red giant branch stars ($P > 70\%$) shows that, if the studied objects were genuine physical systems as old and metal-rich as the Sgr field population, they would be uncovered from their CMDs after the decontamination of field stars, i.e., stars with $P > 70\%$ would appear along the metal-rich red giant branch. Such a metal-rich giant branch would come from the excess of these stars over the Sgr field population, so that no confusion with Sgr field stars would come out.

3.2. Metallicities

We searched the Sloan Digital Sky Survey (SDSS) IV DR16, in particular the APOGEE-2 database (Blanton et al. 2017; Ahumada et al. 2020), for overall metallicities ($[M/H]$) and α -element abundances ($[\alpha/M]$) of stars located within the eight globular clusters discovered by Minniti et al. (2021b) and their respective six star field circles as illustrated in Fig. 1, and applied the proper motions filter of ± 1 mas/yr from the M54's proper motion, as in Section 2. APOGEE-2 spectra were reduced (Nidever et al. 2015) and analyzed using the APOGEE

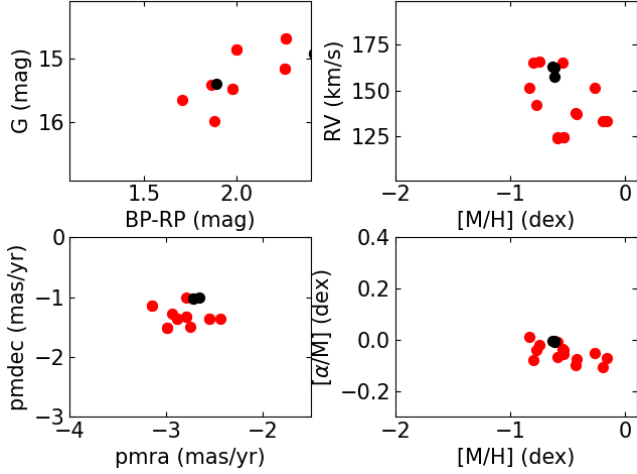


Figure 7. *Gaia* ($G, BP - RP$) CMD (top-left); vector point diagram (bottom-left); radial velocity vs. $[M/H]$ (top-right); and $[M/H]$ vs. $[\alpha/M]$ (bottom-right) for stars located within Minni 335 (black filled symbols) and star field (red filled symbols) circles, respectively, as devised in Fig. 1.

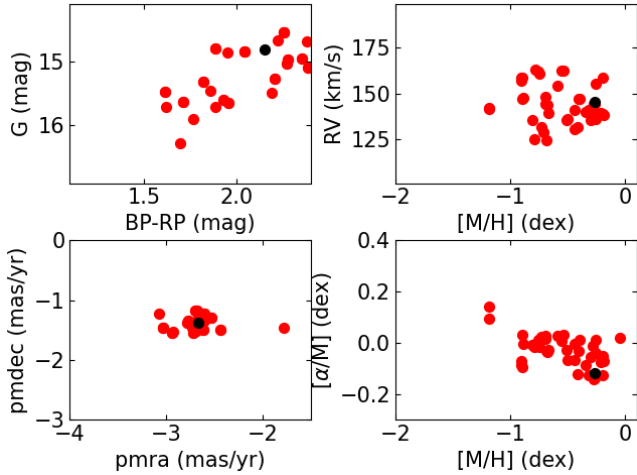


Figure 7. continued: Minni 341.

Stellar Parameters and Chemical Abundance Pipeline (ASPCAP; García Pérez et al. 2016). Particularly, we used the following Structured Query Language (SQL) query to the SDSS database server : ²

```
SELECT TOP 100
s.apogee_id,s.ra,s.dec,s.glon,s.glat,s.snr,
s.vhelio_avg,s.verr,s.gaia_pmra,s.gaia_pmra_error,
s.gaia_pmdec,s.gaia_pmdec_error,
s.gaia_phot_g_mean_mag,s.gaia_phot_bp_mean_mag,
s.gaia_phot_rp_mean_mag,a.teff,a.teff_err,a.logg,
a.logg_err,a.m_h,a.m_h_err,a.alpha_m,a.alpha_m_err
```

² <http://skyserver.sdss.org/dr16/en/tools/search/sql.aspx>

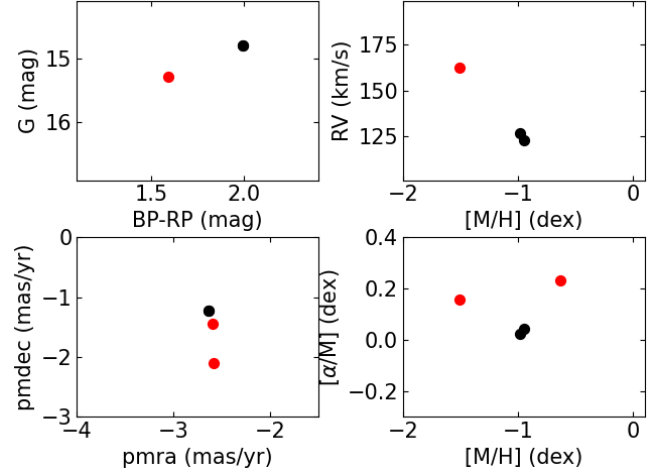


Figure 7. continued: Minni 342.

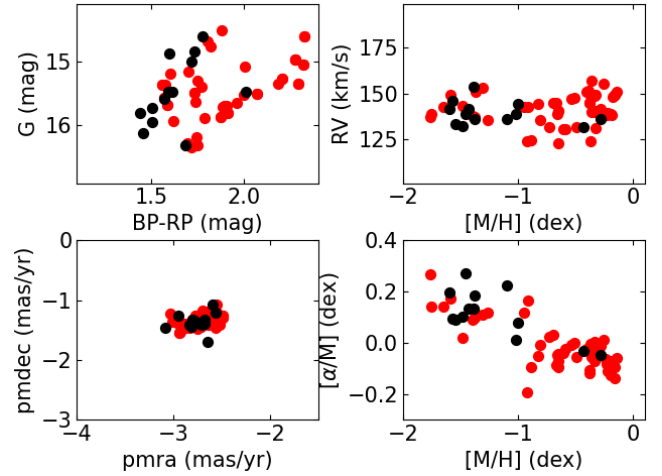


Figure 7. continued: M54.

```
FROM apogeeStar as s
JOIN aspcapStar a on s.apstar_id = a.apstar_id
JOIN dbo.fGetNearbyApogeeStarEq(RA,DEC,3) as
near on a.apstar_id=near.apstar_id
```

```
WHERE (a.aspcapflag & dbo.fApogeeAspcapFlag(
'STAR_BAD')) = 0 and s.commiss = 0
```

Because of the much brighter magnitude limit of APOGEE-2 with respect to *Gaia* EDR3, only very few bright red giants were found for some globular clusters. The lack of a statistically reasonable sample of stars in each globular cluster field makes the subsequent analysis to be considered as complementary to the CMD cleaning procedure. It can be affected by stochastic effects. Indeed, stars found inside the cluster circles can be field stars projected along the line-of-sight. We fortunately found a couple of stars for Minni 335, 341, and 342. For completeness purposes, we carried out a similar search for M54. Fig. 7 shows the different plots drawn from

the gathered information, where black and red filled circles represent stars located within the cluster and star field circles, respectively. Typical uncertainties in the *Gaia* EDR3 G magnitudes, and $BP - RP$ colors for the G magnitude range considered are ~ 0.005 , and 0.100 mag, respectively (Riello et al. 2020), while the mean errors retrieved from APOGEE-2 for the remaining parameters are: $\sigma(pmra) = 0.08$ mas/yr; $\sigma(pmdec) = 0.07$ mas/yr; $\sigma(RV) = 0.02$ km/s; $\sigma([M/H])$ and $\sigma([\alpha/M]) = 0.02$ dex. As can be seen, they are smaller than the size symbols of Fig. 7.

The G versus $BP - RP$ CMDs of Minni 335 shows one star located inside the cluster circle (black symbol in Fig. 7) placed along the broad sequence representing the Sgr field red giant branch population (red symbols). By comparing it with Fig. 4, we found that it has a low P value, similar to those of field stars. Its APOGEE-2 $[M/H]$ value is ~ -0.7 dex, thus confirming that it is more metal-rich than M54. Minni 341 shows a single star that survived the selection criteria and is located within the cluster’s circle. It is brighter and redder than the CMD limits used for the decontamination of field stars. Its metal content ($[M/H] \sim -0.3$ dex) tells us about a much younger star, if the Sgr age-metallicity relationship were taken into account (Kruijssen et al. 2020). Indeed, it would be younger than ~ 1 Gyr, in good agreement with the conclusions drawn from the cleaned CMD. As for Minni 342, the selected stars are at the tip of the red giant branch (see Fig. 4), while their metallicities suggest, by using the Sgr age-metallicity relationship, an age younger than ~ 9 Gyr. The CMD of M54 clearly shows two sequences that correspond to the cluster and to the surrounding star red giant branch or the metal-rich red giants of M54, represented by black and red symbols, respectively. Along the M54’s metal-poor red giant branch there are interlopers, because we did not cleaned the CMD from field contamination. Likewise, along the Sgr field red giant branch there are some stars located in the cluster circle, which can be metal-rich cluster red giant branch stars (see discussion above).

The vector point diagrams of Fig. 7 simply confirm that the selected stars have the same proper motion of M54 within ± 1 mas/yr. For the same kinematics reasons, radial velocities of stars inside cluster circles are among that of M54. As far as the overall metallicity and the α -element abundances are considered, the values for stars located inside cluster circles for Minni 335, 341 and 342 are distributed similarly as Sgr field stars. For M54, the different metallicity regimes –metal-poor for the cluster and metal-rich for the Sgr field stars – and $[\alpha/M]$ ratios are distinguishable. Note that some cluster stars may have also metal-rich overall chemical compo-

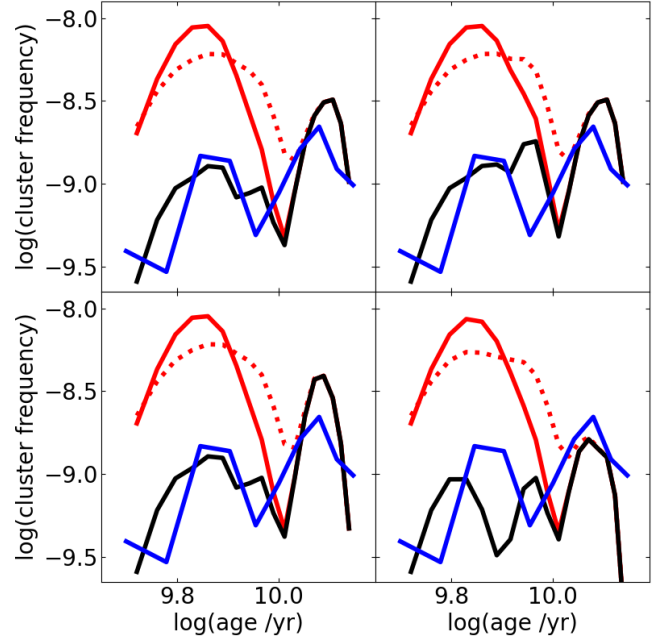


Figure 8. CFs derived from considering the ages of Sgr globular clusters (black line); that computed from the Sgr SFR (blue line), and that built adding 8 globular clusters with an age of 7 ± 1 Gyr (red solid line) or adding 8 globular clusters distributed as follows: $2 \times 6 \pm 1$ Gyr, $2 \times 7 \pm 1$ Gyr, $2 \times 8 \pm 1$ Gyr, $2 \times 9 \pm 1$ Gyr (red dotted line), respectively. The CFs are normalized to the total number of clusters, for comparison purposes. The Sgr globular cluster samples used are those adopted by Massari et al. (2019) and Kruijssen et al. (2020) (top-left panel); Forbes (2020) (top-right panel); Bellazzini et al. (2020) (bottom-left panel); and Arakelyan et al. (2021) (bottom-right panel).

sitions and $[\alpha/M] \lesssim 0.0$ dex, and metal-poor interlopers may also exist. Summing up, the available APOGEE-2 data favor the existence of metal-rich ($[M/H] \geq -1.0$ dex), $[\alpha/M]$ ratios $\lesssim 0.0$ dex, and young stars inside the studied clusters’ circles.

3.3. Sgr cluster frequency

The age distribution of Sgr globular clusters is tightly related to the early galaxy formation history (see, e.g. Kruijssen et al. 2019). It has been shown that the so-called cluster frequency (CF), the number of clusters per time unit as a function of age, is an appropriate tool to describe the cluster formation history, as compared to age histograms (see, e.g. Baumgardt et al. 2013; Piatti 2014; Piskunov et al. 2018). CFs trace the number of clusters per time unit, while histogram bins span different time interval. For instance, a histogram in $\log(\text{age})$ with bin sizes of 0.1 embraces periods of time of ~ 2.6 Myr and ~ 260 Myr at the age intervals of $\log(\text{age}) = 7.0-7.1$ and $9.0-9.1$, respectively. This uneven split of the whole time period produces spurious peaks in the

number of clusters, thus misleading the interpretation about enhanced periods of cluster formation or periods of more intense cluster dissolution.

In order to build the Sgr CF we used the ages of the eight members selected by [Massari et al. \(2019\)](#) and [Kruijssen et al. \(2020\)](#), who provided consistent evidence for considering them purely associated to Sgr (NGC 2419, 5824, 6715, Pal 12, Terzan 7, 8, Arp 2, Whiting 1). Some different globular cluster samples have also been associated by other studies ([Bellazzini et al. 2020](#); [Forbes 2020](#); [Arakelyan et al. 2021](#)) to Sgr. For the sake of the reader, we have also used them in the subsequent analysis. Each age was represented by a one-dimensional *Gaussian* of unity area centered on the respective age value, with a FWHM/2.335 equals to the age error. We added the different *Gaussians* and then computed the integral of the resulting *Gaussian* for adjacent age intervals of 0.5 Gyr wide, from 5.0 up to 14.0 Gyr, to obtain the total number of clusters per age interval. Note that the resulting CF accounts also for the uncertainties in the age estimates (see, Table A1 in [Kruijssen et al. 2019](#)). We refer the reader to the works by [Bagheri et al. \(2013\)](#); [Piatti \(2014\)](#); [Piatti et al. \(2018\)](#), and references therein) for details about the construction of CFs. The resulting CFs are shown in Fig. 8 drawn with black solid line. As can be seen, there have been two main globular cluster formation epochs, at ~ 12.6 and 7.4 Gyr, respectively. Both peaks agree very well with the Sgr star formation history recovered by [de Boer et al. \(2015\)](#). Indeed, we used their Sgr SFR (see their Fig. 6) to build the CF by adopting a power-law cluster mass distribution with slope α ([Salpeter 1955](#); [Kroupa 2002](#); [Gennaro et al. 2018](#)) and assuming that clusters and field stars share the same formation rates (SFR \equiv CF [Lada & Lada 2003](#)). CF and SFR are linked through the expression:

$$CF(t) = SFR(t) \times \frac{\sum m^{-\alpha}}{\sum m^{(-\alpha+1)}} \quad (1)$$

where m is the cluster mass and the sums are computed over the Sgr cluster mass range ($\sim 2 \times (10^3 - 10^6 M_\odot)$; [Baumgardt et al. 2019](#)). Note that the shape of the resulting CF as a function of the cluster age does not depend on the value of the slope α adopted (see Eq. (1).) The blue solid line drawn in Fig.8 represents the CF obtained from the adopted Sgr SFR. The resulting CF follows the overall shape of the CFs directly derived from counts of globular clusters per age interval. This means that both formation processes (clusters and field stars) have taken place concurrently. According to [Minniti et al. \(2021b\)](#), their eight new globular clusters have red giant branches that resemble those of the Sgr metal-rich

star population ($[Fe/H] \gtrsim 1.0$ dex). By considering the Sgr age-metallicity relationship ([Forbes 2020](#); [Kruijssen et al. 2020](#)), this means that they should be younger than 9 Gyr. Taking into account such an age range, we adopted possible age distributions of the eight globular clusters discovered by [Minniti et al. \(2021b\)](#), and built the CFs with these 8 globular clusters added following the above procedure. Fig. 8 illustrates the resulting CFs for two different age distributions, namely: i) 8 globular clusters with an age of 7 ± 1 Gyr; and ii) 8 globular clusters with ages of 6 ± 1 Gyr (2); 7 ± 1 Gyr (2); 8 ± 1 Gyr (2); and 9 ± 1 Gyr (2), depicted with a red solid and dotted lines, respectively. Any other possible age distribution results in a similar CF, which are very different from the expected Sgr CF. Similar analyses on the real number of star clusters in a galaxy from its CF have also carried out by [Piatti](#) (e.g. [2017b](#), [2018b,c](#)). This outcome shows that, if the Sgr globular cluster population included 8 new young members, the resulting CF would result significantly different from that obtained from the known Sgr SFR.

4. CONCLUSIONS

The ancient globular cluster population of a galaxy plays an important role in our understanding of the formation and early evolution of that galaxy. Particularly, the actual number of globular clusters, their age and metallicity distributions are tightly linked with that formation and evolution processes. Recently, [Minniti et al. \(2021b\)](#) discovered eight globular clusters in the Sgr dwarf galaxy from the inspection of optical CMDs filtered from the M54's proper motion, the Sgr nuclear cluster. Such a amazing number of new globular clusters, which is nearly similar to the number of known globular clusters in Sgr is expected to match its cluster frequency and age-metallicity relationship.

In order to prove the genuine physical reality of these new globular clusters, we employed the *Gaia* EDR3 database, following the cuts applied by [Minniti et al. \(2021b\)](#), to additionally clean them later from field star contamination. We used a cleaning procedure that provided membership probabilities for all the measured stars, those with positions, astrometry and photometry in the *Gaia* EDR3 database. We found that most of the stars that survived the cleaning procedure have different membership probabilities. The resulting spatial distributions of stars with membership probabilities higher than 50% showed a clear compact stellar overdensity in the field of Minni 332, whose distributions in the cleaned CMD resemble that of a cluster red giant branch more metal-rich than that of M54. This implies that Minni 332 is also much younger than M54. As a

control of the cleaning procedure and the interpretations of the cleaned CMD, we did the same analysis for M54. We thus uncovered the cluster CMD that is very well reproduced by a theoretical isochrone for the cluster’s age and metallicity.

Two fields, Minni 342 and 348, show some hints for a spatial concentration of stars belonging to the asymptotic and horizontal branches, no other CMD cluster features were possible to be identified. They could be cluster candidates as Minni 349, although the latter does not exhibit any stellar overdensity. Minni 341 resulted to be a possible young cluster candidate (< 1 Gyr), while the analysis of Minni 335, 343 and 344 did not lead us to confirm them as stellar aggregates. Their cleaned CMD show populated red giant branches that coincide with that of the Sgr composite stellar field rather than with the red giant branch of ancient Sgr globular clusters. Additionally, we found that the number of RR Lyrae stars counted by Minniti et al. (2021b) in circles of $3'$ and $10'$ of radius centered on the globular clusters - they have sizes of $1'-2'$ in radius - linearly increase with the distance from the clusters’ centers.

We searched the APOGEE-2 database with the aim of looking for chemical abundances that complement the analysis of the cleaned CMDs. Unfortunately, APOGEE-2 is not deep enough as to reach the bottom of the Sgr red giant branch, but only the tip of the red giant branch. Nevertheless, the retrieved chemical data for stars projected along the line-of-sight of the globular clusters and those of adjacent fields, that have kinematics similar to that of M54, show that stars inside the analyzed clusters’ circles are relatively metal-rich ($[M/H] \geq -1.0$ dex), with $[\alpha/M] \lesssim 0.0$ dex and much younger than the ancient globular clusters. Note that this result come from the analysis of star samples that were not cleaned from the contamination of field stars as we did for the globular clusters’ CMDs.

Finally, we built the Sgr cluster frequency using the ages of different samples of associated globular clusters found in the literature. All the resulting cluster frequencies show a very good agreement with that obtained from the Sgr star formation rate, which confirms that globular clusters and field stars formed concurrently. We then added eight globular clusters with ages between 6 and 9 Gyr, as judged by the Sgr age-metallicity relationship, the implied metallicity from the cleaned CMDs,

and the values provided by APOGEE-2. From any possible combination of ages for eight new Sgr globular clusters, the resulting CFs clearly differentiate from the Sgr star formation rate.

I thank the referee for the thorough reading of the manuscript and timely suggestions to improve it.

This work has made use of data from the European Space Agency (ESA) mission *Gaia* (<https://www.cosmos.esa.int/gaia>), processed by the *Gaia* Data Processing and Analysis Consortium (DPAC, <https://www.cosmos.esa.int/web/gaia/dpac/consortium>). Funding for the DPAC has been provided by national institutions, in particular the institutions participating in the *Gaia* Multilateral Agreement.

Funding for the Sloan Digital Sky Survey IV has been provided by the Alfred P. Sloan Foundation, the U.S. Department of Energy Office of Science, and the Participating Institutions. SDSS acknowledges support and resources from the Center for High-Performance Computing at the University of Utah. The SDSS web site is www.sdss.org.

SDSS is managed by the Astrophysical Research Consortium for the Participating Institutions of the SDSS Collaboration including the Brazilian Participation Group, the Carnegie Institution for Science, Carnegie Mellon University, Center for Astrophysics — Harvard & Smithsonian (CfA), the Chilean Participation Group, the French Participation Group, Instituto de Astrofísica de Canarias, The Johns Hopkins University, Kavli Institute for the Physics and Mathematics of the Universe (IPMU) / University of Tokyo, the Korean Participation Group, Lawrence Berkeley National Laboratory, Leibniz Institut für Astrophysik Potsdam (AIP), Max-Planck-Institut für Astronomie (MPIA Heidelberg), Max-Planck-Institut für Astrophysik (MPA Garching), Max-Planck-Institut für Extraterrestrische Physik (MPE), National Astronomical Observatories of China, New Mexico State University, New York University, University of Notre Dame, Observatório Nacional / MCTI, The Ohio State University, Pennsylvania State University, Shanghai Astronomical Observatory, United Kingdom Participation Group, Universidad Nacional Autónoma de México, University of Arizona, University of Colorado Boulder, University of Oxford, University of Portsmouth, University of Utah, University of Virginia, University of Washington, University of Wisconsin, Vanderbilt University, and Yale University.

REFERENCES

- Ahumada, R., Prieto, C. A., Almeida, A., et al. 2020, *ApJS*, 249, 3, doi: [10.3847/1538-4365/ab929e](https://doi.org/10.3847/1538-4365/ab929e)
- Alfaro-Cuello, M., Kacharov, N., Neumayer, N., et al. 2019, *ApJ*, 886, 57, doi: [10.3847/1538-4357/ab1b2c](https://doi.org/10.3847/1538-4357/ab1b2c)

- Arakelyan, N. R., Pilipenko, S. V., & Sharina, M. E. 2021, arXiv e-prints, arXiv:2105.09850.
<https://arxiv.org/abs/2105.09850>
- Bagheri, G., Cioni, M.-R. L., & Napiwotzki, R. 2013, *A&A*, 551, A78, doi: [10.1051/0004-6361/201118236](https://doi.org/10.1051/0004-6361/201118236)
- Baumgardt, H., Hilker, M., Sollima, A., & Bellini, A. 2019, *MNRAS*, 482, 5138, doi: [10.1093/mnras/sty2997](https://doi.org/10.1093/mnras/sty2997)
- Baumgardt, H., Parmentier, G., Anders, P., & Grebel, E. K. 2013, *MNRAS*, 430, 676, doi: [10.1093/mnras/sts667](https://doi.org/10.1093/mnras/sts667)
- Bellazzini, M., Ibata, R., Malhan, K., et al. 2020, *A&A*, 636, A107, doi: [10.1051/0004-6361/202037621](https://doi.org/10.1051/0004-6361/202037621)
- Bellazzini, M., Ibata, R. A., Chapman, S. C., et al. 2008, *AJ*, 136, 1147, doi: [10.1088/0004-6256/136/3/1147](https://doi.org/10.1088/0004-6256/136/3/1147)
- Blanton, M. R., Bershadsky, M. A., Abolfathi, B., et al. 2017, *AJ*, 154, 28, doi: [10.3847/1538-3881/aa7567](https://doi.org/10.3847/1538-3881/aa7567)
- Bressan, A., Marigo, P., Girardi, L., et al. 2012, *MNRAS*, 427, 127, doi: [10.1111/j.1365-2966.2012.21948.x](https://doi.org/10.1111/j.1365-2966.2012.21948.x)
- de Boer, T. J. L., Belokurov, V., & Koposov, S. 2015, *MNRAS*, 451, 3489, doi: [10.1093/mnras/stv946](https://doi.org/10.1093/mnras/stv946)
- de Boer, T. J. L., Gieles, M., Balbinot, E., et al. 2019, *MNRAS*, 485, 4906, doi: [10.1093/mnras/stz651](https://doi.org/10.1093/mnras/stz651)
- Fernández-Trincado, J. G., Beers, T. C., Minniti, D., et al. 2021, *A&A*, 648, A70, doi: [10.1051/0004-6361/202140306](https://doi.org/10.1051/0004-6361/202140306)
- Forbes, D. A. 2020, *MNRAS*, 493, 847, doi: [10.1093/mnras/staa245](https://doi.org/10.1093/mnras/staa245)
- Gaia Collaboration, Prusti, T., de Bruijne, J. H. J., et al. 2016, *A&A*, 595, A1, doi: [10.1051/0004-6361/201629272](https://doi.org/10.1051/0004-6361/201629272)
- Gaia Collaboration, Luri, X., Chemin, L., et al. 2020, arXiv e-prints, arXiv:2012.01771.
<https://arxiv.org/abs/2012.01771>
- García Pérez, A. E., Allende Prieto, C., Holtzman, J. A., et al. 2016, *AJ*, 151, 144, doi: [10.3847/0004-6256/151/6/144](https://doi.org/10.3847/0004-6256/151/6/144)
- Gennaro, M., Tchernyshyov, K., Brown, T. M., et al. 2018, *ApJ*, 855, 20, doi: [10.3847/1538-4357/aaa973](https://doi.org/10.3847/1538-4357/aaa973)
- Helmi, A., Babusiaux, C., Koppelman, H. H., et al. 2018, *Nature*, 563, 85, doi: [10.1038/s41586-018-0625-x](https://doi.org/10.1038/s41586-018-0625-x)
- Ibata, R., Bellazzini, M., Chapman, S. C., et al. 2009, *ApJL*, 699, L169, doi: [10.1088/0004-637X/699/2/L169](https://doi.org/10.1088/0004-637X/699/2/L169)
- Kroupa, P. 2002, *Science*, 295, 82, doi: [10.1126/science.1067524](https://doi.org/10.1126/science.1067524)
- Kruijssen, J. M. D., Pfeffer, J. L., Reina-Campos, M., Crain, R. A., & Bastian, N. 2019, *MNRAS*, 486, 3180, doi: [10.1093/mnras/sty1609](https://doi.org/10.1093/mnras/sty1609)
- Kruijssen, J. M. D., Pfeffer, J. L., Chevance, M., et al. 2020, *MNRAS*, 498, 2472, doi: [10.1093/mnras/staa2452](https://doi.org/10.1093/mnras/staa2452)
- Lada, C. J., & Lada, E. A. 2003, *ARA&A*, 41, 57, doi: [10.1146/annurev.astro.41.011802.094844](https://doi.org/10.1146/annurev.astro.41.011802.094844)
- Law, D. R., & Majewski, S. R. 2010, *ApJ*, 714, 229, doi: [10.1088/0004-637X/714/1/229](https://doi.org/10.1088/0004-637X/714/1/229)
- Massari, D., Koppelman, H. H., & Helmi, A. 2019, *A&A*, 630, L4, doi: [10.1051/0004-6361/201936135](https://doi.org/10.1051/0004-6361/201936135)
- Minniti, D., Fernández-Trincado, J. G., Gómez, M., et al. 2021a, *A&A*, 650, L11, doi: [10.1051/0004-6361/202141129](https://doi.org/10.1051/0004-6361/202141129)
- Minniti, D., Gómez, M., Alonso-García, J., Saito, R. K., & Garro, E. R. 2021b, arXiv e-prints, arXiv:2106.03605.
<https://arxiv.org/abs/2106.03605>
- Monaco, L., Bellazzini, M., Ferraro, F. R., & Pancino, E. 2005, *MNRAS*, 356, 1396, doi: [10.1111/j.1365-2966.2004.08579.x](https://doi.org/10.1111/j.1365-2966.2004.08579.x)
- Nidever, D. L., Holtzman, J. A., Allende Prieto, C., et al. 2015, *AJ*, 150, 173, doi: [10.1088/0004-6256/150/6/173](https://doi.org/10.1088/0004-6256/150/6/173)
- Ordoñez, A. J., & Sarajedini, A. 2015, *AJ*, 149, 201, doi: [10.1088/0004-6256/149/6/201](https://doi.org/10.1088/0004-6256/149/6/201)
- Piatti, A. E. 2014, *MNRAS*, 437, 1646, doi: [10.1093/mnras/stt1998](https://doi.org/10.1093/mnras/stt1998)
- . 2017a, *ApJL*, 834, L14, doi: [10.3847/2041-8213/834/2/L14](https://doi.org/10.3847/2041-8213/834/2/L14)
- . 2017b, *A&A*, 606, A21, doi: [10.1051/0004-6361/201731246](https://doi.org/10.1051/0004-6361/201731246)
- . 2018a, *MNRAS*, 477, 2164, doi: [10.1093/mnras/sty773](https://doi.org/10.1093/mnras/sty773)
- . 2018b, *MNRAS*, 478, 784, doi: [10.1093/mnras/sty1249](https://doi.org/10.1093/mnras/sty1249)
- . 2018c, *MNRAS*, 475, 2553, doi: [10.1093/mnras/stx3344](https://doi.org/10.1093/mnras/stx3344)
- . 2021, *AJ*, 161, 199, doi: [10.3847/1538-3881/abe545](https://doi.org/10.3847/1538-3881/abe545)
- Piatti, A. E., Aparicio, A., & Hidalgo, S. L. 2017, *MNRAS*, 469, 1175, doi: [10.1093/mnras/stx1002](https://doi.org/10.1093/mnras/stx1002)
- Piatti, A. E., & Bica, E. 2012, *MNRAS*, 425, 3085, doi: [10.1111/j.1365-2966.2012.21694.x](https://doi.org/10.1111/j.1365-2966.2012.21694.x)
- Piatti, A. E., Cole, A. A., & Emptage, B. 2018, *MNRAS*, 473, 105, doi: [10.1093/mnras/stx2418](https://doi.org/10.1093/mnras/stx2418)
- Piatti, A. E., & Fernández-Trincado, J. G. 2020, *A&A*, 635, A93, doi: [10.1051/0004-6361/202037439](https://doi.org/10.1051/0004-6361/202037439)
- Piatti, A. E., Mestre, M. F., Carballo-Bello, J. A., et al. 2021, arXiv e-prints, arXiv:2101.01818.
<https://arxiv.org/abs/2101.01818>
- Piskunov, A. E., Just, A., Kharchenko, N. V., et al. 2018, ArXiv e-prints. <https://arxiv.org/abs/1802.06779>
- Riello, M., De Angeli, F., Evans, D. W., et al. 2020, arXiv e-prints, arXiv:2012.01916.
<https://arxiv.org/abs/2012.01916>
- Salpeter, E. E. 1955, *ApJ*, 121, 161, doi: [10.1086/145971](https://doi.org/10.1086/145971)
- Vasiliev, E., & Baumgardt, H. 2021, arXiv e-prints, arXiv:2102.09568. <https://arxiv.org/abs/2102.09568>